COMMUNICATION

Interface passivation to overcome shunting in semiconductor-catalyst junctions†

Cite this: DOI: 10.1039/c9cc09597g

Parisa Shadabipour and Thomas W. Hamann D*

Received 10th December 2019, Accepted 27th January 2020

DOI: 10.1039/c9cc09597g

rsc.li/chemcomm

10

50

High-performance mesoporous hematite photoanodes modified with a conductive water oxidation catalyst, $Ni_{0.75}Fe_{0.25}O_xH_{yr}$, for photoelectrochemical water oxidation are limited by shunting. We present a general method to overcome shunting *via* the selective electrodeposition of a thin poly(phenylene oxide) (PPO) insulating layer onto the exposed transparent conductive oxide substrate prior to catalyst deposition.

Photoelectrochemical (PEC) water splitting with semiconductor materials is a widely studied approach to convert and store solar energy in carbon-free fuels. 1-3 The oxidative half-reaction (OER) is generally the bottleneck of the overall water splitting process. Thus, there has been intense effort over the past decade to develop efficient and robust photoanode materials to enhance the efficiency of PEC water oxidation. In recent years, the integration of water oxidation catalysts (WOCs) with photoanodes has been an extensively reported route to improve their performance.⁵⁻⁹ The use of WOCs for boosting the performance of photoanodes have been successfully demonstrated through various suggested mechanisms, including enhanced charge separation, 10,11 an increase of band bending, 12,13 and surface passivation. 14,15 However, the overall PEC activity of the WOC-modified photoanodes are dictated not only by the catalyst composition but also the structural features of the photoanode. In some cases, the integration of WOCs are actually detrimental to the performance of certain photoanodes. For instance, the efficiency of mesoporous BiVO4 and hematite photoanodes, widely studied for PEC OER, showed a significant decrease upon modification with the conductive WOCs, such as Co-Pi, NiOOH, and Ni(Fe) O_xH_v (Ni-rich). 16-19 An increase in the rate of carrier recombination at the catalyst/

Department of Chemistry, Michigan State University, 578 South Shaw Lane, East Lansing, Michigan 48824-1322, USA

† Electronic supplementary information (ESI) available: Experimental sections and additional characterization including scanning electron microscopy, Raman spectroscopy, scanning transmission electron microscopy, elemental mapping and, cyclic voltammetry measurements. See DOI: 10.1039/c9cc09597g

photoanode interface has been put forth as an explanation for the deteriorated performance of these systems.

Recently, Boettcher and coworkers used dual working electrode (DWE) measurements to show the decrease in the PEC performance of mesoporous hematite upon addition of Ni(Fe)O_rH_v catalysts is due to the introduction of a new shunting recombination pathway between the transparent conductive oxide (TCO) substrate and the conductive catalyst. 18 The porosity of the photoanode layer deposited onto TCOs is therefore an important, but generally overlooked, design parameter for realizing efficient PEC water splitting. Indeed, the occurrence of such shunting recombination in many prior reports of mesoporous photoelectrodes can also be inferred based on findings of performance improvement by (i) increasing the photoanode thickness, ¹⁹ (ii) improving the surface morphology (e.g., fabrication of a pinhole-free photoanode using atomic layer deposition (ALD)), 16 and (iii) the inclusion of an additional non-conductive catalyst layer.6 Mesoporous photoanodes, however, are particularly attractive because of their high aspect ratios and from simple fabrication methods, such as electrodeposition or spray pyrolysis. Therefore, developing approaches to effectively eliminate shunting in porous photoelectrodes, without compromising the morphological characteristics, is critical to achieving high performance. This issue is not widely appreciated for PEC water splitting, however, and methods to overcome shunting are lacking in the literature.

In this work, hematite photoanodes were prepared through the electrodeposition from 0.1 M $FeCl_2 \cdot 4H_2O$ solutions onto fluorine-doped tin oxide (FTO) substrates (ED-hematite hereafter). Such hematite photoanodes have been previously reported to have a mesoporous morphology and thus serve as an excellent platform to evaluate the effect of shunting and methods to overcome it. As a result of the mesoporous structure, there are areas of the FTO substrate which are in direct contact with the solution when immersed in the electrolyte. The exposure of the FTO to the electrolyte for the mesoporous ED-hematite films was elucidated by comparing the dark cyclic voltammetric (CV) response to that of bare FTO

Q1

10

5

15

20

25

30

35

40

45

50

55

Communication ChemComm

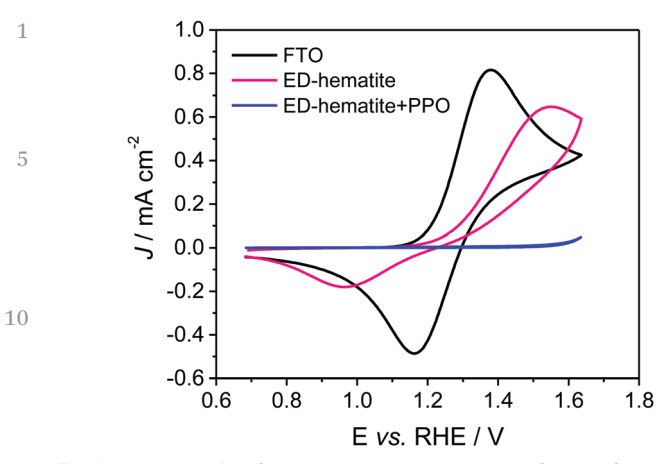


Fig. 1 The role of PPO on insulating the exposed FTO. Dark CV response of the bare FTO (black), ED-hematite (pink) and PPO-modified ED-hematite (blue) in 1.0 M KOH containing 10 mM $\rm K_4[Fe(CN)_6]$ solution. Scan rate is 10 mV s⁻¹.

electrodes in a 10 mM ferri/ferrocyanide (hole scavenger) solution (Fig. 1). A reversible redox wave appears on the bare FTO (black line in Fig. 1), which corresponds to charge transfer between the ferri/ferrocyanide and the conductive electrode. A similar reversible redox wave, albeit with a smaller peak height and increased peak separation, is also observed for the EDhematite (pink line in Fig. 1), which indicates that a portion of the FTO remains exposed to the electrolyte after hematite electrodeposition. It is important to note that it is not feasible to identify this exposed FTO through the hematite layer by inspection of scanning electron micrographs of the hematite film (Fig. S1a and b, ESI†). However, the presence of pinholes in the ED-hematite layer was identified through cross-sectional imaging of the sample using high-angle annular dark-field scanning transmission electron micrograph (HAADF-STEM) and energy-dispersive X-ray (EDX) analysis (Fig. 2 and also see Fig. S2, ESI†).

Since ferri/ferrocyanide redox couples can penetrate the hematite film, we reasoned that organic monomers can likewise penetrate hematite films and contact the FTO substrate and be selectively polymerized to form an insulating film. We, therefore, introduced solutions containing phenol and 2-allylphenol, which were anodically electropolymerized to form

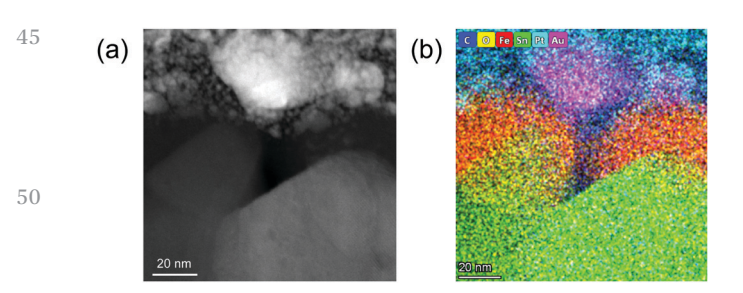


Fig. 2 HAADF-STEM and EDX elemental mapping of the PPO-modified ED-hematite. (a) HAADAF-STEM image and (b) EDX mapping overlay of tin (green), iron (red), oxygen (yellow), carbon (blue), platinum (cyan), and gold (pink).

poly(phenylene oxide) (PPO) insulating films following the previous procedure (Fig. S3, ESI \dagger). The self-limiting growth mechanism results in very thin (\sim 12 nm) films of PPO being produced selectively of the FTO substrates. The insulating nature of the electrodeposited PPO prevents the direct charge transfer between the FTO layer and ferri/ferrocyanide species, which is evidenced by the lack of a redox wave for this system (blue line in Fig. 1). The absence of the ferri/ferrocyanide redox wave after treating the ED-hematite with PPO suggests that PPO sufficiently covers all the exposed FTO and a pinhole-free film is obtained. This can also be confirmed from the comparison of X-ray photoelectron spectroscopy (XPS) measurements of bare and PPO modified ED-hematite (Fig. S4, ESI \dagger).

1

5

10

15

2.0

25

30

35

40

45

50

5.5

In order to determine the extent of any unwanted electropolymerization of PPO on hematite, we also attempted to deposit PPO on the hematite photoanode prepared via atomic layer deposition (ALD). ALD yields a pinhole-free hematite thin film as previously determined²¹ and further evidenced by dark CV measurements in ferri/ferrocyanide solution (Fig. S5, ESI†). Following the same electropolymerization conditions with the ALD-hematite electrodes resulted in essentially no current attributed to electropolymerization which contrasts the behavior of bare FTO and ED-hematite (Fig. S6, ESI†). Importantly, we found that modification of the ED-hematite photoanode with PPO does not compromise the performance of the EDhematite photoanode for water oxidation. Fig. S7a (ESI†) compares the performance of the pristine and PPO-modified ED hematite for the PEC OER, where the measured current remains identical. Similarly, we observed identical performance for the pinhole-free ALD-hematite before and after PPO electrodeposition (Fig. S7b, ESI†). These observations suggest that PPO deposition is unlikely to occur on the hematite surface.

In order to assess the effect of shunting to catalysts by exposed FTO, $Ni_{0.75}Fe_{0.25}O_xH_y$ electrocatalysts were integrated with ED-hematite photoanodes. This catalyst composition was chosen because the Ni-rich phase is known for its high electrical conductivity compared to the Fe-rich phase, and it is amongst the most active known water oxidation catalysts in basic media. 22,23 Fig. 3a shows the dark and light current density vs. applied potential (*J-E*) responses of a typical EDhematite electrode in contact with 1.0 M KOH aqueous electrolyte before and after deposition of a smooth ~ 220 nm thick $Ni_{0.75}Fe_{0.25}O_xH_v$ electrocatalyst (see Fig. S8 and the explanation in the ESI† for the characterization of the catalyst thickness). The deposition of $Ni_{0.75}Fe_{0.25}O_xH_y$ results in a very large dark current along with the appearance of cathodic peaks at 1.3 V (vs. RHE) under both dark and illumination conditions. This peak, which also appears when the catalyst is directly deposited on bare FTO, corresponds to the reduction of Ni³⁺ to Ni²⁺ on exposed FTO, and thus suggests a direct contact between the conductive catalysts and the FTO layer underneath the hematite (Fig. S9, ESI†).18 This shunting from the direct contact between catalyst and substrate severely deteriorates the PEC performance of the ED-hematite photoanode compared to the unmodified electrode. Notably, an additional redox wave

ChemComm Communication

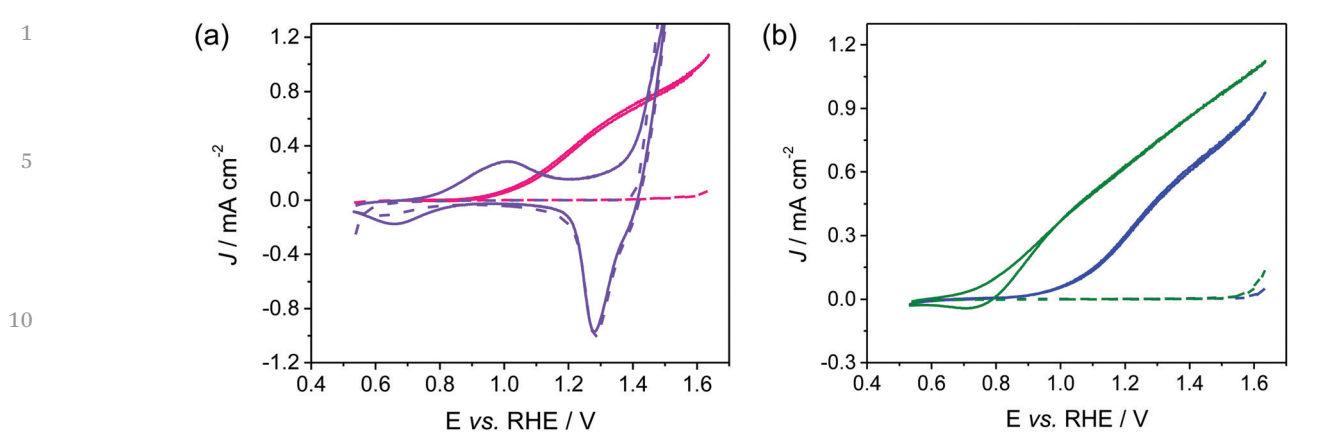
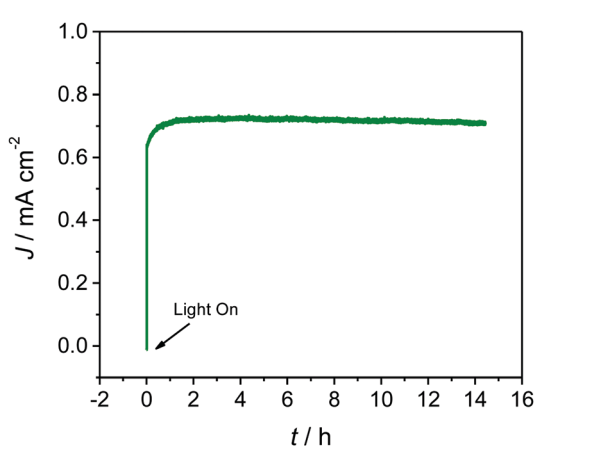


Fig. 3 Impact of PPO electrodeposition on the elimination of shunting recombination (a) J-E curves of the bare ED-hematite under illumination (solid pink line), in the dark (dashed pink line) and after deposition of $Ni_{0.75}Fe_{0.25}O_xH_y$ catalyst under illumination (solid violet line) and in the dark (dashed violet line). (b) J-E curves of ED-hematite after electrodeposition of PPO under illumination (solid blue line), in the dark (dashed blue line) and after deposition of $Ni_{0.75}Fe_{0.25}O_xH_y$ under illumination (solid green line) and in the dark (dashed green line). All measurements were done in 1.0 M KOH, the scan rate of 10 mV s⁻¹.

centered at 0.8 V (νs . RHE) also appears upon illumination of the catalyst modified-photoanode. This peak is also related to the Ni³⁺/Ni²⁺ redox couple but occurs at the hematite surface. The generation of photovoltage in hematite under illumination resulted in about 0.5 V cathodic shift of Ni³⁺/Ni²⁺ redox wave on the hematite surface compared to the same redox process on exposed FTO. Similar observations were previously reported where porous semiconductors were modified with an electrically conductive catalyst such as CoPi and Ni_{0.8}Fe_{0.2}O_xH $_y$. ^{18,19}

Fig. 3b shows the *J–E* behavior of ED-hematite electrodes with PPO blocking layers in contact with 1.0 M KOH aqueous electrolyte. As noted above, the addition of the PPO film does not affect the PEC performance without a catalyst. There is a striking difference in performance upon the deposition of a Ni_{0.75}Fe_{0.25}O_xH_y electrocatalyst, however. Once the shunting pathway has been passivated through the addition of the PPO layer, there is no significant dark current and the reduction peak on FTO (Ni3+ to Ni2+ at 1.3 V vs. RHE) is eliminated. Blocking the shunting pathway also results in a significant improvement in the PEC performance, where a ~200 mV cathodic shift of the photocurrent onset potential is observed on the catalyst-deposited electrode compared to the bare electrode along with a significant increase in the photocurrent density. This improved behavior is similar to the improvement reported many times for compact hematite electrodes with a variety of catalysts, which is now well understood. 10,17,18

Hematite is well known for its exceptional stability photoelectrochemical in a basic environment. He meantime the PPO layers are also expected to be stable under anodic conditions; indeed they are deposited by applying potentials significantly more positive than expected at the hematite photoelectrode surface. In order to determine the robustness of the PPO layer under PEC water splitting conditions, we measured the photocurrent for the ED-hematite + PPO $|Ni_{0.75}$ - $Fe_{0.25}O_xH_y$ photoanode in 1.0 M KOH under 1 sun illumination at a constant applied potential of 1.26 V vs. RHE (Fig. 4). The measured photocurrent density of 0.72 mA cm $^{-2}$ shows



1

10

15

20

25

30

35

40

45

50

55

Fig. 4 Photostability measurement of ED-hematite + PPO $|Ni_{0.75}$ -Fe $_{0.25}O_xH_y$ for PEC OER. J-t plot measured at 1.26 V vs. RHE in 1.0 M KOH under 1 sun illumination.

remarkable stability over 15 hours of measurement, proving the long-term stability of the PPO layer with no sign of photobleaching or degradation under the measurement conditions.

In summary, in this work we introduced a simple, general approach to eliminate shunting by direct contact of electrocatalysts with conductive substrates through selective electrodeposition of PPO into a porous photoelectrode. The shunting, while its degree depends on photoelectrode morphology and catalyst conductivity, can severely limit the performance in PEC processes. We demonstrate that the integration of PPO results in a pronounced improvement in the performance of ED-hematite|Ni_{0.75}Fe_{0.25}O_xH_y for PEC OER with remarkable stability. This approach should generally be applicable to other photoelectrode systems for improving their efficiencies in solar-energy applications, an open area for future research.

T. W. H. is grateful to the NSF for support of this work by Award CHE-1664823. We acknowledge the Michigan Center for Materials Characterization for staff assistance and use of the instruments. Communication ChemComm

Conflicts of interest

There are no conflicts to declare.

Notes and references

10

2.5

30

35

40

- M. G. Walter, E. L. Warren, J. R. McKone, S. W. Boettcher, Q. Mi, E. A. Santori and N. S. Lewis, *Chem. Rev.*, 2010, 110, 6446–6473.
- 2 S. Chu, W. Li, Y. Yan, T. Hamann, I. Shih, D. Wang and Z. Mi, *Nano Futures*, 2017, **1**, 022001.
- 3 Y. He, T. Hamann and D. Wang, Chem. Soc. Rev., 2019, 48, 2182-2215.
- 4 B. M. Hunter, H. B. Gray and A. M. Müller, *Chem. Rev.*, 2016, **116**, 14120–14136.
- 5 J. Deng, X. Lv, H. Zhang, B. Zhao, X. Sun and J. Zhong, *Phys. Chem. Chem. Phys.*, 2016, 18, 10453–10458.
- 6 T. W. Kim and K.-S. Choi, Science, 2014, 343, 990-995.
- 7 S. D. Tilley, M. Cornuz, K. Sivula and M. Grätzel, *Angew. Chem., Int. Ed.*, 2010, **49**, 6405–6408.
- 8 J. Qiu, H. Hajibabaei, M. R. Nellist, F. A. L. Laskowski, T. W. Hamann and S. W. Boettcher, ACS Cent. Sci., 2017, 3, 1015–1025.
- and S. W. Boettcher, *ACS Cent. Sci.*, 2017, 3, 1015–1025.

 9 J. W. Jang, C. Du, Y. Ye, Y. Lin, X. Yao, J. Thorne, E. Liu, G. McMahon,
- J. Zhu, A. Javey, J. Guo and D. Wang, *Nat. Commun.*, 2015, 6, 7447.
 B. Klahr, S. Gimenez, F. Fabregat-Santiago, J. Bisquert and T. W. Hamann, *J. Am. Chem. Soc.*, 2012, 134, 16693–16700.
- 11 G. M. Carroll and D. R. Gamelin, J. Mater. Chem. A, 2016, 4, 2986–2994.
- 12 M. Barroso, A. J. Cowan, S. R. Pendlebury, M. Grätzel, D. R. Klug and J. R. Durrant, *J. Am. Chem. Soc.*, 2011, **133**, 14868–14871.

- 13 M. Barroso, C. A. Mesa, S. R. Pendlebury, A. J. Cowan, T. Hisatomi, K. Sivula, M. Gratzel, D. R. Klug and J. R. Durrant, *Proc. Natl. Acad. Sci. U. S. A.*, 2012, **109**, 15640–15645.
- 14 R. Liu, Z. Zheng, J. Spurgeon and X. Yang, Energy Environ. Sci., 2014, 7, 2504–2517.
- 15 C. Zachäus, F. F. Abdi, L. M. Peter and R. Van De Krol, Chem. Sci., 2017, 8, 3712–3719.
- 16 G. M. Carroll, D. K. Zhong and D. R. Gamelin, Energy Environ. Sci., 2015, 8, 577–584.
- 17 H. Hajibabaei, A. R. Schon and T. W. Hamann, *Chem. Mater.*, 2017, 29, 6674–6683.
- 18 J. Qiu, H. Hajibabaei, M. R. Nellist, F. A. L. Laskowski, S. Z. Oener, T. W. Hamann and S. W. Boettcher, ACS Energy Lett., 2018, 3, 961–969
- 19 M. R. Nellist, J. Qiu, F. A. L. Laskowski, F. M. Toma and S. W. Boettcher, ACS Energy Lett., 2018, 3, 2286–2291.
- 20 B. A. Gregg, F. Pichot, S. Ferrere and C. L. Fields, J. Phys. Chem. B, 2001, 105, 1422–1429.
- 21 B. M. Klahr, A. B. F. Martinson and T. W. Hamann, *Langmuir*, 2011, 27, 461–468.
- 22 L. Trotochaud, S. L. Young, J. K. Ranney and S. W. Boettcher, J. Am. Chem. Soc., 2014, 136, 6744–6753.
- 23 D. A. Corrigan, J. Electrochem. Soc., 2006, 134, 377.
- 24 K. Sivula, F. Le Formal and M. Grätzel, ChemSusChem, 2011, 4, 432-449.
- 25 A. G. Tamirat, J. Rick, A. A. Dubale, W.-N. Su and B.-J. Hwang, *Nanoscale Horiz.*, 2016, 1, 243–267.
- 26 P. Dias, A. Vilanova, T. Lopes, L. Andrade and A. Mendes, *Nano Energy*, 2016, 23, 70–79.

25

1

10

15

20

40

45

50

55

30

35

45

50

55